Polymer Chemistry

Accepted Manuscript

ROYAL SOCIETY OF CHEMISTRY

www.rsc.org/polymers

Polymer Chemistry

RSCPublishing

ARTICLE

Synthesis and characterization of perfluoro-*tert*-butyl semifluorinated amphiphilic polymers and their potential application in hydrophobic drug delivery.

Cite this: DOI: 10.1039/xoxxoooooox

Received ooth,
Accepted ooth

DOI: 10.1039/xoxxoooooox

www.rsc.org/

Sarah Decato,[a] Troy Bemis,[a] Eric Madsen[a] and Sandro Mecozzi[b]

Semifluorinated polymer surfactants, composed of a monomethyl poly(ethylene glycol) (mPEG) hydrophilic head group and either 1, 2, or 3 perfluoro-*tert*-butyl (PFtB) groups as the fluorophilic tail, were synthesized, and their aqueous self-assemblies were investigated as a potential design for theranostic nanoparticles. Polymers with three PFtB groups ($PFtB_{TRI}$) solely formed stable, spherical micelles, approximately 12 nm in size. These $PFtB_{TRI}$ surfactants demonstrate similar characteristics with those of polymers with linear perfluorocarbon tails, despite large differences in tail structure. For example, PFtB polymer solutions stably emulsified 20 v/v% sevoflurane with perfluorooctyl bromide (PFOB) as a stabilizer. However, these PFtB polymers have the additional potential to serve as F-MRI contrast agents. $PFtB_{TRI}$ micelles gave one narrow ^{19}F-NMR signal in D_2O, with T_1 and T_2 parameters of approximately 500 and 100 ms, respectively. ^{19}F-MR images of PFtB polymer solutions at 1 mM gave intense signal at 4.7 T without sensitizers or selective excitation sequences. These preliminary data demonstrate the potential of PFtB polymers as a basic design, which can be further modified to serve as dual drug-delivery and imaging vehicles.

Introduction

Self-assembly of amphiphilic polymers in aqueous solution provides unique opportunities for multifunctional drug-delivery.[1] Assembly structure can be readily modulated through amphiphile design to provide a variety of sizes and shapes according to the desired application.[2] Stable assemblies in aqueous solution can encapsulate or emulsify hydrophobic drugs via non-covalent hydrophobic interactions. Encapsulation or emulsification by nanoassemblies is crucial for the safe and effective delivery of most hydrophobic drugs—such as antimicrobials and anti-cancer agents—which can exhibit low solubilities in blood[3] and are prone to aggregation[4] and to acute systemic toxicity when administered as a neat solution.[5]

Spherical micelle assemblies, ranging from approximately 10-100 nm in size, are distinctively poised to efficiently deliver chemotherapeutics. Their small size allows them to utilize the enhanced permeation and retention (EPR) effect, which describes the preferential accumulation of such sized particles in tumor tissue via leaky blood vessels.[6]

[a] Department of Chemistry, University of Wisconsin - Madison, Madison, Wisconsin 53706.

[b] School of Pharmacy, University of Wisconsin – Madison, Madison Wisconsin 53705.

† Electronic Supplementary Information (ESI) available: MALDI-MS, ^{1}H ^{19}F and ^{13}C NMR spectra. TEM image and T_1 and T_2 relaxation curves.

The rapid development of vasculature to support prolific cancer growth results in larger endothelial gaps in the blood vessels, allowing drug nanocarriers to accumulate preferentially within tumor tissue. Increasing the *in vivo* circulation time of the drug-polymer assembly enhances this passive targeting of the tumor cells.[7] Unfortunately, many non-covalent aggregates will rapidly dissociate in blood due to interactions with hydrophobic blood components.[8] Previous work in our laboratory has demonstrated that the installation of a perfluorinated segment into an amphiphile can provide prolonged circulation time by deterring hydrophobic interactions with blood components and by increasing the inherent stability of the aggregates. Due to this enhanced *in vivo* stability of the drug-polymer assembly, arising from the fluorous block, semifluorinated drug-carriers have the potential for controlled and sustained release of encapsulated hydrophobic molecules.[9]

The structure of semifluorinated polymers can be readily modified to serve as a multifunctional nanoparticle drug delivery system. The strategic design and instalment of symmetrical fluorinated tails in such polymers allows for the development of dual therapeutic and imaging contrast agents, i.e., theranostic agents, for simultaneous drug delivery and imaging of labeled particles *in vivo*.[10] Magnetic resonance imaging (MRI) is a non-invasive, deeply penetrating, non-

destructive imaging modality that provides unparalleled tissue contrast. Specially designed contrast agents allow for site- or pathology-specific images, i.e. molecular images that can be overlaid with anatomical images.[11] The ^{1}H nucleus is best suited for anatomical imaging due to the abundance of water in the body and can also function as a molecular imaging nucleus when paramagnetic contrast sensitizers such as chelated-Gd^{III} or superparamagnetic iron oxide (SPIO) are applied.[12] These metal-based contrast agents provide indirect imaging of affected nearby water molecules. However, there has been some concern involving the potential toxicity of these compounds. Certain SPIO formulations have demonstrated altered gene expression, oxidative stress, and other biological side-effects,[13] and Gd^{III} has been shown to be particularly toxic in patients with renal deficiency[14].

For direct molecular imaging with low endogenous background signal, the best alternative nucleus for molecular MRI is ^{19}F. It has near-zero background *in vivo*, high gyromagnetic ratio, 100% natural abundance, and is compatible with current MRI instrumentation.[15] The fundamental semifluorinated polymer design has the potential to not only provide enhanced stability as a self-assembly but also serve as a potential label for ^{19}F-MRI. Small molecule perfluorocarbons,[16] particularly perfluoropolyether (PFPE)[17,18] and perfluorooctylbromide (PFOB),[19] have been investigated extensively for this purpose.[20] An alternative approach is to covalently install a fluorinated group in which all fluorine atoms are NMR equivalent to give rise to a single ^{19}F-NMR. This will minimize loss in signal intensity resulting from dipolar interactions between neighboring fluorine atoms and protons, and from broadening of ^{19}F peaks due to the sensitivity of the ^{19}F chemical shift of each CF_2 unit.[21] NMR equivalent fluorine groups will maximize signal-to-noise ratios (SNR) without application of selective excitation sequences.

After considering NMR equivalent fluorine concentration, the next major parameter to consider in contrast agent design is relaxation time. The resulting assemblies must exhibit short spin-lattice (T_1) and long spin-spin (T_2) values to maintain high signal intensity. In dynamic systems, such as micelle self-assemblies, the T_2 relaxation time is particularly prone to shortening, resulting in significant loss in signal intensity. In a study by Nyström *et al.* no ^{19}F signal could be detected from an aqueous assembly when a fluorinated segment was installed within a rigid hydrophobic core.[22] Following studies by Peng *et al*. demonstrated that self-assemblies with more fluid cores allowed for increased ^{19}F signal.[23] A recent approach was developed by Whittaker *et al.* in which charged monomer units were utilized to increase mobility of the fluorinated segment.[24] These studies demonstrate the importance of careful consideration of nanoparticle design to maximize image sensitivity while maintaining surface-active properties for self-assembly.

In this study an alternative approach is employed to increase mobility, or increase fluidity, of the fluorinated segment by using a branched architecture, which provides frustrated packing. Typically when contrast agents are installed in the core of the assembly the signal intensity is dramatically reduced. However, branched structures reduce interactions between non-equivalent fluorine atoms, which reduces the loss of contrast from dipolar interactions between nuclear spins.[25] The perfluoro-*tert*-butyl (PFtB) moiety was selected as it is highly branched and has demonstrated good characteristics as a general ^{19}F-MRI contrast agent, ^{19}F-Imaging Tracer (^{19}FIT).[26] The modularly symmetrical ^{19}FIT molecule is composed of a branched PEG hydrophilic head group with amide linkages and a tail consisting of three PFtB groups. Aqueous solutions of these molecules exhibited a single ^{19}F signal even as aggregates. Additionally, they showed no acute toxicity *in vivo* with a residence half-life of approximately 0.5 days in mice and no evidence of organ retention or *in vivo* degradation. These studies demonstrate the PFtB's advantageous properties for *in vivo* imaging contrast. However, the ^{19}FIT molecule was designed for general contrast and therefore is not directly amenable to serve as a theranostic particle for molecular imaging. Also the extent of the surface-active properties of PFtB polymers had not previously been rigorously investigated.

Described in this article are the self-assembly physicochemical properties of semifluorinated polymers in aqueous solution arising from the introduction of one or multiple PFtB moieties. The potential application of these self-assemblies as molecular ^{19}F-MR imaging contrast agents is also confirmed. The basic amphiphilic polymer design is composed of a fluorous tail, which is modularly increased in fluorophilicity to include 1, 2, and 3 PFtB groups ($PFtB_{MONO}$, $PFtB_{DI}$, and $PFtB_{TRI}$, respectively) and a hydrophilic monomethyl poly(ethylene glycol) (mPEG) head group. The mPEG length is relatively small (1,000 and 2,000 g/mol average molecular weight) in order to provide aqueous solubility and prolonged evasion from blood clearance by the mononuclear phagocyte system (MPS) while maximizing the percent fluorine per molecule, which is directly proportional to ^{19}F signal intensity. Our results demonstrate that the PFtB group, when properly installed in an amphiphilic polymer, can drive the self-assembly of small, stable micelles in aqueous media and provide contrast for ^{19}F-MR imaging. The proposed polymers serve as a foundation for a multifunctional unimer design that can be modulated to include other intermediate blocks for hydrophobic drug or dye encapsulation. The surface can also be readily decorated with fluorophores, positron emission tomography (PET) radioisotopes, or other contrast labels for multi-modality imaging. Additionally, site-specific targeting ligands may also be conjugated to the assembly surface to increase bioaccumulation and cell uptake of drug-containing nanocarriers to specific tissue.[27] The versatile multifunctional amphiphile design described herein demonstrates the potential for PFtB-based polymers to serve as effective theranostic particles,[28] capable of monitoring the fate of colloidal drug systems *in vivo* including cell uptake[29] and biodistribution.[30]

Experimental

Materials and Methods. 1H,1H-perfluorotetradecanol was purchased from SynQuest Laboratories Inc. (Alachua, FL). Perfluoro-*tert*-butanol was purchased from Matrix Scientific (Columbia, SC). Rabbit red blood cells (10%, 15 mL) were purchased from Lampire Biological Laboratories Inc. (Pipersville, PA). All other reagents and solvents were purchased from Sigma Aldrich Co. (Milwaukee, WI) and used as received, unless otherwise specified. Small molecule and polymer chromatographic separations were performed using Silicycle 60 Å SiO_2 or using a Combi-flash Rf 200 (Teledyne ISCO, Lincoln, NE) equipped with ELSD for compound visualization using REDI-Sep Rf Gold high performance silica cartridges.

^1H, ^{19}F, and ^{13}C NMR spectra were obtained on Varian Unity-Inova 400 or Unity-Inova 500 spectrometers using $CDCl_3$ as the solvent with trimethylsilane (TMS) as an internal reference at 25 °C unless otherwise specified. Polymer purity was analyzed by HPLC with a Gilson 321 Pump (Middleton, WI) equipped with a Jordi Gel DVB 500 Å column (Bellingham, MA) and a Gilson Prep-ELS detector and by MALDI-MS on a Bruker Ultraflex III MALDI TOF/TOF using α-cyano-4-hydroxycinnamic acid (CHCA) matrix unless otherwise specified.

Critical micelle concentration (CMC). The appropriate polymer was dissolved in Milipore Milli-Q water (equipped with a 0.22 μm filter) in a 20 mL disposable scintillation vial to the desired maximum concentration (dependent upon the solubility of the polymer in water and upon the available quantity of polymer). The solution was then shaken, sonicated for 20 min, and allowed to equilibrate for 24 hours. (If bubbles were still present after this time, the solution was allowed to continue to equilibrate until all bubbles had dissipated.) Serial dilutions were then prepared from this stock solution to achieve the desired concentrations, again allowing for each dilution to equilibrate before subsequent dilution. After all dilutions were prepared, they were allowed to equilibrate for an additional 24 hours. A custom round platinum rod, with a diameter of 1.034 mm with a wetted length of 3.248 mm from KSV Instruments, (Helsinki, Finland) was cleaned with ethanol and dried in a Bunsen burner flame. The surface tension of Millipore water was measured first and the value confirmed to be within ± 2 mN/m of the literature value (72.8 mN/m). The surface tension of each vial was then measured using the Wilhelmy method, beginning with the least concentrated, at room temperature (r.t.) on a KSV sigma 701 tensiometer from KSV Instruments (Helsinki, Finland) equipped with a Schott Titronic Universal dispenser for automatic CMC measurements and a Julabo F12-MC circulator for constant temperature control. Each sample was measured in quadruplicate and the average recorded. The CMC value was determined from the intersection of the slope at the crossover point and the slope at high concentrations. The error in the CMC measurement was calculated by applying a weighted least squares analysis to the linear sections of interest. The individual uncertainties of the two slopes and intercepts produced by the weighted least squares analysis were then propagated through as follows:

$$x_{Log(M)} = \frac{b_2 - b_1}{m_1 - m_2}$$

$$\sigma_{x_{Log(M)}} = \sqrt{x_{Log(M)}^2 \left[\left(\frac{\sigma_{b_2 - b_1}}{b_2 - b_1} \right)^2 + \left(\frac{\sigma_{m_1 - m_2}}{m_1 - m_2} \right)^2 \right]}$$

Where:

$$\sigma_{m_1 - m_2} = \sqrt{\sigma_{m_1}^2 + \sigma_{m_2}^2} \qquad \sigma_{b_2 - b_1} = \sqrt{\sigma_{b_2}^2 + \sigma_{b_1}^2}$$

The weighted least squares analysis was chosen because the uncertainty of each individual data point was known, yielding insight into the precision of the CMC calculation.

Dynamic light scattering (DLS). Samples were prepared by direct dilution of the polymer in Milli-Q water to the desired concentration. Particle sizes of polymer solutions were analyzed by dynamic light scattering using a NICOMP 380ZLS from Particle Sizing Systems (Santa Barbara, CA) without further dilution in Plastibrand 1.5 mL PS semi-micro disposable cuvettes from Sigma Aldrich Co. (Milwaukee, WI). Each sample was measured before and after filtration with a 4 mm dia., 0.45 μm nylon syringe filter from Thermo Fisher Scientific Inc. (Fitchburg, WI). Each particle size analysis was performed at r.t. and repeated in triplicate with the number of scans of each run determined automatically by the instrument according to the concentration of the solution. The data was analyzed using NICOMP analysis and reported as volume weighted average diameters. Error was reported as the standard deviation of the particle diameter as reported by the NICOMP software.

Transmission electron microscopy (TEM). The polymer solution was prepared by direct dilution in Milli-Q water. Due to poor contrast in aqueous samples, 4 μL of solution was pipetted onto the lacey carbon grid from Electron Microscopy Sciences (Hatfield, PA) and dried for 10 s under a heat lamp. The grids were imaged using the Technai T-12 Cryo TEM operating at 120 kV. Images were taken with a Gatan Ultrascan CCD camera with resolution of 2048 x 2048 pixels. Image provided in supplementary information.

Microviscosity. Polymer solutions of 0.2 $mmolL^{-1}$ in acetonitrile and 1,3-bis-(1-pyrenyl)propane (P3P) solution of 2.7 $ngmL^{-1}$ in chloroform were prepared. Micelle solutions were then prepared via the solvent evaporation method: 1 mL of polymer solution and 67 μL of the P3P solution were added to a 25 mL round-bottom flask. The samples were heated to 60 °C and rotated on the rotary evaporator without vacuum for 5 min. The samples were then condensed under reduced pressure for 15 min while rotating, allowed to cool for 5 min, and then dispersed with 1 mL of 60 °C phosphate buffered saline (PBS). The samples were shaken vigorously and then filtered with a 4 mm dia., 0.45 μm nylon filter and stored in amber vials. The

fluorescence analysis was carried out on an AMINCO-Bowman Series 2 spectrometer from Thermo Fisher Scientific (Fitchburg, WI) with excitation at 333 nm, emission at 378 nm, and a spectral window of 350 – 500 nm. Error was reported as the standard deviation from triplicate measurements.

Electrostatic potential energy surface (EPS) calculations. Calculations were performed using *Spartan'10* from Wavefunction Inc. (Irvine, CA). The surfaces were generated by mapping 6-31G** electrostatic potentials onto surfaces of molecular electron density (0.002 electron/Å) and color-coding. In all surfaces, the potential energy values range from +150 kcal/mol to -150 kcal/mol, with red signifying a value greater than or equal to the maximum in negative potential and blue signifying a value greater than or equal to the maximum in positive potential.

Emulsions. Polymer solutions were prepared by direct dilution of lyophilized solid in sterile, normal saline solution to a total volume of 11.9 mL. The solutions were sonicated until completely dissolved. A 3.4 mL volume of Sevoflurane from Abbott Labs (N. Chicago, IL) and 1.7 mL of perfluorooctyl bromide from SynQuest Laboratories, Inc. (Alachua, FL) were added to the polymer solution via a 1 mL Eppendorf pipet for a total volume of 17 mL. The high-speed homogenizer (Power Gen 500) from Fisher Scientific (Hampton, NH) and the microfluidizer (model 110 S) from Microfluidics Corp. (Newton, MA) were first cleaned with 70 % and 100 % ethanol, followed by 70 % and 100 % methanol, and finally with three rinses of Millipore water. Once prepared the mixture was then homogenized with the high-speed homogenizer for 1 min at 21000 rpm at r.t. The crude emulsion was then microfluidized for 1 min at 5000 psi with the cooling bath kept at 10 °C. The final emulsion was then filtered with a 30 mm dia., 0.45 μm nylon filter and stored in 45 mL plastic centrifuge tubes from Corning Inc. (Corning, NY) at 4 °C. After preparation and filtration of the emulsions, the emulsion droplet sizes were measured by dynamic light scattering (NICOMP 380ZLS) from Particle Sizing Systems (Santa Barbara, CA). An aliquot of the emulsion, approximately 25 μL, was diluted in 3 mL of Milipore water to achieve an intensity factor range of 300-350. Each measurement was run for 5 minutes at r.t. and repeated in triplicate. The data was analyzed using Gaussian analysis and reported as a volume-weighted average diameter. The emulsion errors for all polymers were taken as an average of the standard deviations of each individual measurement. The standard deviation of the average error for the reported polymers was 14.73 nm (minimum error: 21.16 and maximum error: 71.68) with the exception of $mPEG_{2k}OPFtB_{MONO}$ (minimum error: 19.73 and maximum error: 246.64). The average particle size standard deviation was then used to determine the uncertainty in the Ostwald ripening rate data as follows

$$OstwaldRipeningRate = \frac{dr^3}{dt}$$

$$F(r) = r^3$$

So if:

$$\sigma_{F(r)}^2 = \left(\frac{dF}{dr}\right)^2 \sigma_r^2 = \left(3r^2\right)^2 \sigma_r^2$$

Then:

$$\sigma_{F(r)} = 3r^2 \sigma_r$$

For emulsions that exhibited linearity, a weighted least squares analysis was performed to best show the Ostwald ripening rate trend. The analysis provides the Ostwald ripening rate, as well as the uncertainty of the linear fit. These errors have not been plotted for clarity but the average uncertainty in the slope for reported polymers that exhibited linearity was on the order of $6E^4$.

Hemolysis Assay. Polymer solutions ($mPEG_{1k}$-$OPFtB_{MONO}$ and $mPEG_{1k}$-$OPFtB_{TRI}$) were made by direct dilution in sterile PBS. Suspended rabbit red blood cells (10%, 15 mL) were centrifuged (2000 rpm, 2 min, 25 °C, 450 g), the supernatant was removed, and the cells were resuspended in 15 mL of sterile PBS. To each well of a clear 96-well plate was added varying amounts of rabbit red blood cells and (100 – x) μL of sterile PBS buffer, where x represents the amount of rabbit red blood cells (10, 20, 50, and 100 μL) that was added to the respective well. Each experimental condition was repeated in triplicate. Finally, 100 μL of the appropriate polymer solution was added to each well. The plates were incubated statically at 37°C for 3 h. The plates were then centrifuged to pellet the cells (4 min, 25 °C, 450 g). A 100 μL portion of supernatant from each well of culture was transferred to a fresh, clear 96-well plate. Absorbance at 420 nm and 540 nm was measured for each well using a plate reader and percent hemolysis was determined. Complete hemolysis of the positive control was achieved by treating red blood cells with 100 μL of Milli-Q water in place of polymer solution.

Magnetic resonance imaging (MRI). Samples were prepared by direct dilution to achieve 10 mM concentration in D_2O with TMS as an internal standard. Micelle formation was confirmed by DLS. The temperature was maintained at 25°C. The ^{19}F relaxation parameters, T_1 and T_2 measurements of the micelles, were conducted on a Varian Unity-Inova 400 MHz spectrometer. The T_1 was determined using an inversion recovery experiment acquired with 12 independent, quadratically spaced variable (tau) values covering a range up to 5 times the estimated T_1, 0.4 s. The T_2 was determined using a Carr-Purcell-Meiboom-Gill, CPMG, pulse sequence experiment acquired with 12 independent, quadratically spaced variable (tau) values covering a range up to 5 times the estimated T_2, 0.4 s. For T_1 and T_2 measurements: 90° pulse = 13.4 μs, nt = 4, spectral window (T_1) = 21575.0 Hz and spectral window (T_2) = 15763.5 Hz.

MRI images were acquired using a Varian 4.7 T small animal scanner using a home-built ^{19}F quadrature volume coil with a 1.5 '' diameter and 3 '' in length. The temperature was maintained at 26 °C. A polymer stock solution of $mPEG_{1k}$-$OPFtB_{TRI}$ was prepared by direct dilution of lyophilized solid polymer sample to the highest phantom concentration in Milli-

Q water. Lower phantom concentrations were made as serial dilutions from the stock solution in Milli-Q water. Micelle formation was confirmed by DLS. Phantom polymer solutions; 5 mM, 1 mM, 0.1 mM, 0.01 mM, and 0 mM, were transferred to Teflon-free glass vials and ^{1}H images of the phantoms were acquired using a gradient echo pulse sequence with 0.3 × 0.3 × 2.0 mm^3 spatial resolution, 32 × 32 mm^2 field-of-view (FOV), 0.1 s TR, 2.12 ms TE, 20° flip angle, 350 Hz/pixel bandwidth, 8 averages and 1 min 17 sec imaging time. ^{19}F images of the phantoms were acquired using a spin echo pulse sequence with a 1.0 × 1.0 × 2.0 mm^3 spatial resolution, 32 × 32 mm^2 FOV, 2 s TR, 6 ms TE, 32 echoes, 1050 Hz/pixel bandwidth, 24 averages, and 25 min 36 sec imaging time. Images were summed along the echo dimension to increase SNR efficiency by taking advantage of the long T_2.

Synthesis

"mPEG$_x$-OMs" Monomethyl polyethyleneoxide mesylate. In a typical reaction, to a solution of mPEG$_x$-OH (2.5 mmol) in DCM (anhydrous, 30 mL) under argon was syringed triethylamine (0.87 mL, 6.25 mmol), followed by MsCl (0.39 mL, 5 mmol). The solution was stirred as it warmed to r.t. and was allowed to stir overnight. After this time, the reaction mixture was washed with NH_4Cl_{aq} (2 x 50 ml), brine (50 ml), dried over $MgSO_4$, filtered, and the solvent reduced to 10 mL *in vacuo*. The product was precipitated with diethyl ether at 0 °C (~250 mL) and collected by filtration. The precipitate was redissolved in DCM (50 mL) and the volume was reduced to ~10 mL *in vacuo*. Benzene was added to the solution (~10 mL), which was then frozen in an acetone/dry ice bath and dried overnight *in vacuo*. Note one must keep the polymer cold and work quickly with smaller mPEG polymers, which have low melting points. ***mPEG$_{550}$-OMs**:* Yield 85%. ^{1}H NMR ($CDCl_3$, 400 MHz): δ 4.39-4.37 (m, 2H), 3.83-3.81 (m, 1H), 3.78-3.76 (m, 2H), 3.64 (m, 47H), 3.56-3.54 (m, 2H), 3.47 (m, 1H), 3.38 (s, 3H), 3.09 (s, 3H). ***mPEG$_{1k}$-OMs**:* Yield 94%. ^{1}H NMR ($CDCl_3$, 400 MHz): δ 4.39-4.37 (m, 2H), 3.83-3.81 (m, 1H), 3.78-3.75 (m, 2H), 3.64 (m, 89H), 3.56-3.54 (m, 2H), 3.48-3.45 (m, 1H), 3.38 (s, 3H), 3.09 (s, 3H). ***mPEG$_{2k}$-OMs**:* Yield quantitative. ^{1}H NMR ($CDCl_3$, 400 MHz): δ 4.39-4.37 (m, 2H), 3.83-3.81 (m, 2H), 3.78-3.76 (m, 4H), 3.64 (m, 160H), 3.56-3.54 (m, 2H), 3.48-3.45 (m, 2H), 3.38 (s, 3H), 3.08 (s, 3H).

"KOPFtB" Potassium perfluoro-tert-butoxide. According to procedure by Rábai *et al*.,[30] KOH was diluted in 25 mL of deionized water (6.542 g, 0.12 mol) and to this solution was added (25.01 g, 0.11 mol) perfluoro-*tert*-butyl alcohol with stirring at 0°C. The reaction was allowed to stir for 3 h, after which the reaction mixture stirred for an additional 30 min at r.t. The pH of the clear reaction mixture was confirmed to be < 8 and then concentrated *in vacuo*. The white solid was allowed to dry in a desiccator over drierite for two days with a quantitative yield (note that residual KOH may still be present). {^{1}H} NMR (CDCl3,100 MHz): δ 123.1 (q, J = 294.8 Hz, (CF_3), 79.8 (decet, J = 29.9Hz ($C(CF_3)_3$), 68.8 (CH_2), 68.5 (CH). ^{19}F NMR (400 MHz, $CDCl_3$): δ -75.28 (s).

"PFtB$_{MONO}$" series synthesis: mPEGx-OPFtB$_{MONO}$. In a typical reaction, to a solution of mPEG$_x$-OMs (0.48 mmol) in dioxane (2.5 mL), KPFtB (0.72 mmol) was added. The reaction mixture was stirred under Ar at 90 °C for 2 h. The reaction was monitored by HPLC and once complete the reaction was cooled to r.t. The reaction mixture was taken up in DCM, quenched and washed with sat. NH_4Cl_{aq}, dried over $MgSO_4$, and the solvent was reduced *in vacuo*. The product was then precipitated from the organic phase with ether at 0°C and isolated by filtration. The solid was dissolved in 5 mL of DCM and 5 mL of benzene was added, which was then frozen in a dry-ice/acetone bath and dried overnight *in vacuo*. **mPEG$_{550}$-OPFtB$_{Mono}$**: Yield 81 %. ^{1}H NMR ($CDCl_3$, 400 MHz): δ 4.15 (t, J = 4.8Hz, 2H), 3.83-3.82 (m, 1H), 3.73 (t, J = 5.2Hz, 2H), 3.64 (m, 58H), 3.59 (s, 1H), 3.55-3.54 (m, 2H), 3.47-3.45 (m, 1H), 3.38 (s, 3H). ^{19}F NMR (400 MHz, $CDCl_3$): δ -70.78 (s). MALDI MS Performed on a Fourier Transform Mass Spectrometer (Varion-902 MS) equipped with MALDI. $[M+Na]^+$ calcd. for $C_{35}H_{63}F_9O_{16}Na^+$ = 933.39; found: 933.37. **mPEG$_{1k}$-OPFtB$_{Mono}$**: Yield 71 %. ^{1}H NMR ($CDCl_3$, 400 MHz): δ 4.15 (t, J = 4.8Hz, 2H), 3.83-3.81 (m, 1H), 3.74-3.72 (m, 2H), 3.64 (m, 90H), 3.55 (m, 2H), 3.48-3.45 (m, 1H), 3.38 (s, 3H). ^{19}F NMR (400 MHz, $CDCl_3$): δ -70.78 (s). MALDI MS: $[M+Na]^+$ calcd. for $C_{49}H_{91}F_9O_{23}Na^+$ = 1241.57; found: 1241.5. **mPEG$_{2k}$-OPFtB$_{Mono}$**: Yield 70 %. ^{1}H NMR ($CDCl_3$, 400 MHz): δ 4.15 (t, J = 4.8Hz, 2H), 3.83-3.81 (m, 1H), 3.74-3.72 (m, 3H), 3.64 (m, 160H), 3.56-3.54 (m, 2H), 3.48-3.45 (m, 1H), 3.38 (s, 3H). ^{19}F NMR (400 MHz, $CDCl_3$): δ -70.78 (s). MALDI MS: $[M+Na]^+$ calcd. for $C_{95}H_{183}F_9O_{46}Na^+$ = 2254.17; found: 2255.9.

"PFtB$_{DI}$-OH"1,3-bis(1,1,1,3,3,3-hexafluoro-2-(trifluoromethyl)propan-2- yloxy)propan-2-ol. According to Szabó *et al*.,[31] a stirred mixture of 1,3- dribromopropan-2-ol (0.39 mL, 3.95 mmol) and potassium perfluoro-*tert*-butoxide (2.64 g, 9.64 mmol) in dry DMF (10 mL) was heated to 120 °C under argon for 20 h. Water (20 mL) and ether (10 mL) were added, and the aqueous phase was separated and extracted with ether. The organic layers were then combined, washed with water, dried over $MgSO_4$, and filtered. The solvent was removed *in vacuo* and the residue was distilled to afford the product as a colorless, viscous oil (bp 74-79 °C/2.67kPa) with a yield 56 %. ^{1}H NMR ($CDCl_3$, 400 MHz): δ 4.13 - 4.06 (m, 5H), 2.50 (bs, 1H, OH). ^{13}C{^{1}H} NMR (CDCl3, 100 MHz): δ 120.3 (q, J = 294.8Hz, (CF_3), 79.8 (decet, J = 29.9Hz ($C(CF_3)_3$), 68.8 (CH_2), 68.5 (CH). ^{19}F NMR ($CDCl_3$, 400 MHz): δ -71.40 (s).

"PFtB$_{DI}$" series synthesis. mPEG$_x$-OPFtB$_{DI}$: In a typical reaction, at 0 °C was added NaH (3.78 mmol) to a suspension of PFtB$_{DI}$-OH (1.9 mmol) in 15 mL of dry THF under argon. This was allowed to stir for 30 min at 0 °C. After this time, mPEG$_x$-OMs (1.26 mmol) was added at 0 °C. The reaction mixture was allowed to stir as the mixture warmed slowly to r.t.

The reaction mixture was then refluxed until determined to be complete by HPLC. The reaction mixture was then diluted with DCM, quenched and washed with sat. NH_4Cl_{aq}, dried over $MgSO_4$, and concentrated to 10 mL *in vacuo*. The crude product was then precipitated from the organic phase with ether in a dry-ice/acetone bath. The solid was isolated by filtration and then dissolved in 5 mL of DCM. Benzene (5 mL) was added, which was then frozen in dry-ice/acetone bath and dried overnight *in vacuo*. The crude product was purified using the Combi-flash purification system with a C-18 reverse phase Silica column using a Water/MeOH (0.1% FA) to DCM/MeOH gradient. The reaction mixtures containing $mPEG_x$-$OPFtB_{DI}$ and $mPEG_x$-$OPFtB_{MONO}$ could not be purely resolved.

(1-methyl-2,6,7-trioxa-bicyclo[2.2.2]octan-4-yl)methanol (1). In a typical reaction, pentaerythritol (1.98 g, 14.5 mmol) and *p*-toluenesulfonic acid (28 mg, 0.15 mmol) were combined and suspended in 25 mL of dry toluene and heated to reflux (~125 °C) with a dean stark trap and condenser under Ar. To the refluxing reaction mixture was added triethylorthoacetate (2.7 mL, 14.7 mmol). The reaction mixture was allowed to reflux for approximately 24 h until the solution became clear with no visible solid particles. Once complete, 8 drops of triethylamine were added and the reaction mixture was filtered while hot. The solution was then concentrated *in vacuo* with a quantitative yield. ^{1}H NMR ($CDCl_3$, 400 MHz): δ 4.00 (s, 6H, CH_2), 3.44 (d, J = 4.8Hz, 2H, CH_2), 1.73 (t, J = 4.8Hz, 1H, OH), 1.44 (s, 3H, CH_3). ^{13}C{^{1}H} NMR ($CDCl_3$, 100 MHz): δ 108.9, 69.4, 61.4, 35.6, 23.3.

2-(hydroxymethyl)-2-(((4-methoxybenzyl)oxy)methyl)propane-1,3-diol (2). In a typical reaction, KOH pellets were crushed to a powder (2.929 g, 51.45 mmol) and added to stirring dry DMSO (20 mL) at r.t. The suspension was allowed to stir for 5 min. Then **1** was added (1.648 g,, 10.29 mmol) followed quickly by *p*-methoxybenzyl chloride (2.06 mL, 15.22 mmol). The reaction mixture was allowed to stir for 2.5 h. The reaction mixture was then diluted with water (100 mL) and extracted with diethyl ether, washed with brine and water, dried over $MgSO_4$, and concentrated to a white solid *in vacuo*. The residue was dissolved in methanol (40 mL) and treated with 0.01 M HCl (26 mL) at r.t. and was allowed to stir for 1 h. To this was then added 0.967 g of $NaHCO_3$ and was stirred for an additional 1 h. The reaction mixture was then concentrated *in vacuo*. To the residue was added 5 mL of MeOH and filtered. The oil was collected and concentrated *in vacuo*. The residue was purified by flash chromatography on silica gel with 10:6:1 EtOAc:Cyclohexane:MeOH to yield 53 %. ^{1}H NMR ($CDCl_3$, 400 MHz): δ 7.23 (d, J = 8.8 Hz, 2H), 6.89 (d, J = 8.8 Hz, 2H), 4.44 (s, 2H), 3.81 (s, 3H), 3.71 (s, 6H), 3.48 (s, 2H), 2.52 (bs, 3H, OH). ^{13}C{^{1}H} NMR ($CDCl_3$, 100 MHz): δ 159.5, 130.0, 129.5, 114.1, 73.6, 72.2, 64.2, 55.5, 45.3.

"$PFtB_{TRI}$-OPMB" (3). In the optimized reaction, **2** (2.5 g, 9.7 mmol) was added to a (60 mL) pressure round bottom flask with 25 mL of dry THF. To this was added triphenylphosphine (11.52 g, 43.92 mmol), followed by 4 Å MS (2.5 g, powdered and previously activated at 280 °C *in vacuo*) and cooled to 0°C under argon with stirring. Once cooled, (8.88 g, 43.92 mmol) DIAD was added with a glass syringe dropwise. After the addition, the mixture was allowed to stir for approximately 30 min as it warmed to r.t. After this time, (10.37 g, 43.92 mmol) of perfluoro-*tert*-butanol was added with a glass syringe in one portion and the vessel was quickly sealed. The reaction mixture was allowed to stir at 60°C with the Teflon cap screwed onto the sealed vessel for 3 days. After this time, 20 mL of water was added and allowed to stir for 10 min. The reaction mixture was allowed to cool to r.t. and the solvent was removed *in vacuo*. The residue was redissolved in ether and filtered through packed Celite. The filtrate was washed with brine, dried over $MgSO_4$, filtered, and concentrated *in vacuo*. The residue was then purified with the Combi-flash purification system with a normal-phase silica Gold column using a 0-10% EtOAc/Hexanes gradient to yield 63 %. ^{1}H NMR ($CDCl_3$, 400 MHz): δ 7.18 (d, J = 8.8 Hz, 2H), 6.88 (d, J = 8.8 Hz, 2H), 4.38 (s, 2H), 4.04 (s, 6H), 3.81 (s, 3H), 3.40 (s, 2H). ^{13}C{^{1}H} NMR ($CDCl_3$, 100 MHz): δ 159.7, 129.6, 120.3 (q, J = 278.6 Hz, (CF_3), 113.9, 79.9 (decet, J = 30.1 Hz ($C(CF_3)_3$), 73.6, 65.6, 65.2, 55.3 46.4. ^{19}F NMR (400 MHz, CDCl3): δ -71.84 (s).

"$PFtB_{TRI}$-OH". To a stirring mixture of **3** (2.0 g, 2.23 mmol) in 12 mL of THF/H_2O (9:1, v:v) was added ceric ammonium nitrate (CAN) (4.94 g, 8.93 mmol) under argon at r.t. The mixture was then refluxed with vigorous stirring. The reaction was monitored by TLC and was found to be complete after 1 h and 15 min. After this time the reaction mixture was diluted with sat. $NaHCO_3$, extracted with ether, and dried over $MgSO_4$, and concentrated under vacuum for only 1 min. The final compound should only have minimal exposure to vacuum since the product was found to sublime under high vacuum. The crude residue was then purified with the Combi-flash purification system with a normal-phase silica Gold column using a 0-10% EtOAc/Hexanes gradient to give 59 % yield. ^{1}H NMR (CD_3COCD_3, 400 MHz): δ 4.50 (t, J = 1.6 Hz, 1H, OH), 4.25 (s, 6H), 3.71 (d, J = 1.6 Hz, 2H). ^{13}C{^{1}H} NMR (CD_3COCD_3, 100 MHz): δ 120.4 (q, J = 300.0 Hz, (CF_3), 79.7 (decet, J = 28.6Hz ($C(CF_3)_3$), 66.4, 57.5, 46.9. ^{19}F NMR (400 MHz, CD_3COCD_3): δ -71.51 (s).

"$PFtB_{TRI}$" series synthesis: $mPEG_x$-$OPFtB_{TRI}$. In a typical reaction at 0 °C was added NaH (1.26 mmol) to a suspension of $PFtB_{TRI}$-OH (0.63 mmol) in 10 mL of dry THF under argon. This was allowed to stir for 30 min at 0 °C. After this time, $mPEG_x$-OMs (0.32 mmol) was added at 0 °C. The reaction mixture was allowed to stir as the mixture warmed slowly to r.t. The mixture was then refluxed and monitored by HPLC. When determined to be complete the reaction mixture was then diluted with DCM, quenched and washed with sat. NH_4Cl_{aq}, dried over $MgSO_4$, and concentrated to 10 mL *in vacuo*. The crude product was then precipitated from the organic phase with ether in a dry-ice/acetone bath. The solid

was isolated by filtration and then dissolved in 5 mL of DCM and 5 mL of benzene, which was then frozen in dry-ice/acetone bath and dried overnight *in vacuo*. The crude product was purified with the Combi-flash purification system with a C-18 reverse phase Silica column using a Water/MeOH (0.1% FA) to DCM/MeOH gradient. **$mPEG_{1k}$-$OPFtB_{TRI}$**: Yield 56%. ^{1}H NMR ($CDCl_3$, 400 MHz): δ 4.05 (s, 6H), 3.83-3.81 (m, 1H), 3.66-3.54 (m, 96 H), 3.48-3.47 (m, 1H), 3.45 (s, 2H), 3.38 (s, 3H). ^{19}F NMR ($CDCl_3$, 400 MHz): δ -70.82 (s). MALDI MS: $[M+Na]^+$ calcd. for $C_{66}H_{107}F_{27}O_{28}Na^+$ = 1883.64; found: 1883.5. **$mPEG_{2k}$-$OPFtB_{TRI}$**: Yield 59%. ^{1}H NMR ($CDCl_3$, 400 MHz): δ 4.05 (s, 6H), 3.83-3.81 (m, 1H), 3.66-3.54 (m, 167H), 3.47-3.45 (m, 1H), 3.45 (s, 2H), 3.38 (s, 3H). ^{19}F NMR ($CDCl_3$, 400 MHz): δ -70.84 (s). MALDI MS: $[M+Na]^+$ calcd. for $C_{102}H_{179}F_{27}O_{46}Na^+$ = 2676.11; found: 2675.6.

Results and Discussion

Synthesis of semifluorinated polymers. Synthesis of the $PFtB_{MONO}$-terminated polymers was carried out by direct substitution of the mPEG mesylate by the potassium salt of the perfluoro-*tert*-butyl alcohol according to the procedure described by Rábai, *et al.*[31], **Scheme 1** and **Scheme 2**. These reactions were straightforward and high-yielding, with relatively short reaction times. The resulting compounds were very soluble in water and therefore amenable to forming aqueous nano-assemblies.

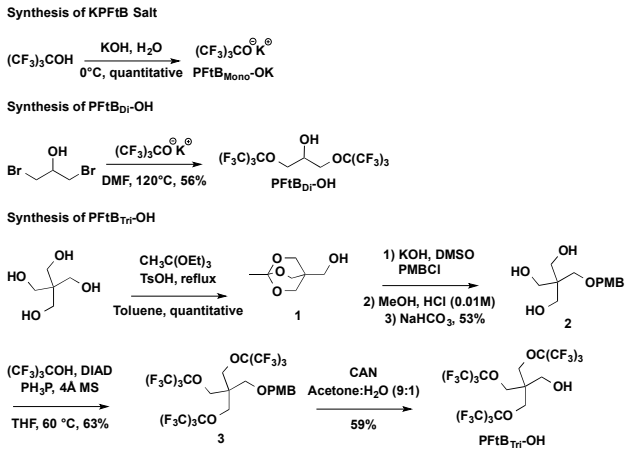

Scheme 1: The synthesis of $PFtB_{MONO}$-OK and $PFtB_{DI}$-OH, are achieved according to previous literature procedures.[30-31] The $PFtB_{TRI}$-OH is achieved by modification a previous literature procedure[33] for small-scale reaction conditions.

The $PFtB_{DI}$ polymer series presented several difficulties but provided keen insight into bioorthogonal fluoropolymer design. The $PFtB_{DI}$ alcohol was synthesized in refluxing DMF and purified by vacuum distillation according to the synthesis described by Nemes *et al.*[32] The volatility and limited solubility of the resulting alcohol made it difficult to separate from the DMF solvent without significant loss of the product under vacuum. The alcohol was also difficult to visualize by TLC despite the hydroxyl functionality. Most importantly, the $PFtB_{DI}$ alcohol is prone to decomposition under subsequent basic reaction conditions, which had been similarly demonstrated in the synthesis of a PFtB containing peptide.[33] Elimination of the β-hydrogen resulted in the release of the PFtB oxide, which readily reacted via substitution with the mPEG mesylate to form the $mPEG_xOPFtB_{MONO}$ polymer. A mixture of the $mPEG_xOPFtB_{MONO}$ and $mPEG_xOPFtB_{DI}$ polymers was evident by MALDI-MS and by NMR, which approximated the compounds to be present in a 9:1 ratio, respectively. These two polymers can be isolated up to approximately 95% purity via flash chromatography without significant loss in yield. However, the significant decomposition of the $PFtB_{DI}$ alcohol indicates that the $mPEG_xOPFtB_{DI}$ may also be prone to degradation. Therefore, a biocompatible fluoropolymer design should avoid β-hydrogens adjacent to the PFtB oxide, which would be detrimental if eliminated *in vivo*.

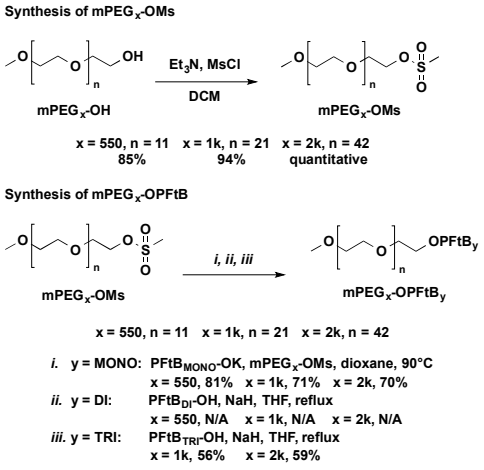

Scheme 2: The synthesis of $mPEG_x$-$OPFtB_{MONO}$, $mPEG_x$-$OPFtB_{DI}$, and $mPEG_x$-$OPFtB_{TRI}$ semifluorinated polymers by substitution of $mPEG_x$-OMs by the corresponding PFtB alcohol synthesized in Scheme 1. N/A signifies that the desired product could not be purely resolved from a reaction side-product, $mPEG_x$-$OPFtB_{MONO}$.

The $mPEG_xOPFtB_{TRI}$ polymer series was more challenging to synthesize. Nevertheless, it provides the largest percent fluorine possible from a single fluorous tail, while maintaining a robust design that can avoid decomposition. The synthesis of the $PFtB_{TRI}$ alcohol was modified from the synthesis by Yu *et al*[34] for small-scale reaction conditions. The steric hindrance and electron withdrawing character of the PFtB groups necessitated vigorous Mitsunobu reaction conditions to afford the desired tri-substituted pentaerythritol, **3**. Adjustments to heat and reaction time had little effect compared to the concentration of the reaction mixture. A *p*-methoxybenzyl (PMB) protecting group was used in lieu of more robust groups, such as the benzyl functionality due to difficulty in deprotection. It should also be noted that the resulting $PFtB_{TRI}$ alcohol, once deprotected, sublimed under vacuum at room temperature and was difficult to visualize by standard TLC stains. Purification was therefore achieved using a Combi-Flash system equipped with an evaporative light scattering detector (ELSD) while minimizing exposure to vacuum. However, as suggested in a similar synthesis from Yu *et al.*,[33] purification from large-scale synthesis may be achieved by simple phase

separation. The resulting $mPEG_{1k}$-$OPFtB_{TRI}$ and $mPEG_{2k}$-$OPFtB_{TRI}$ polymers were sparingly soluble in water. Solutions exceeding 5 mM were extremely viscous, approaching gelification. Since the desired application of the polymers was to form aqueous self-assemblies, the $mPEG_{550}$-$OPFtB_{TRI}$ was not synthesized, as this decrease in the hydrophilic block would further decrease the aqueous solubility of the polymer.

Preparation and characterization of polymer nanoassemblies. Each polymer CMC was measured by surface tension using the Wilhemy method. A reference compound, which has been thoroughly characterized in the literature,[35] $mPEG_{2k}$DSPE 1,2-distearoyl-sn-glycero-3-phosphoethanolamine-N-[methoxy(polyethylene glycol)-2000], was purchased and analysed to provide comparison to these distinct triphyllic polymer surfactants.

The corresponding CMC value for each polymer was then used as the lower limit for all future assembly studies. Of the synthesized PFtB polymers, the $mPEG_x$-$OPFtB_{TRI}$ polymers solely demonstrated typical micelle behavior with a clear sigmoidal curve and a CMC value below log(M) = -3 (or 1 mM), as seen in **Table 1**. The $PFtB_{MONO}$ polymer was not adequately fluorophilic to drive self-assembly of the unimers into regular aggregates.

Semifluorinated polymer	CMC (log(M))	Particle Size (nm)[a]
$mPEG_{550}$-$OPFtB_{MONO}$	N/A[b]	4.4 ± 1.2 (99.9 %), 134.6 ± 61.4 (0.1 %)
$mPEG_{1k}$-$OPFtB_{MONO}$	N/A[b]	68.9 ± 35.8 (100 %)
$mPEG_{2k}$-$OPFtB_{MONO}$	N/A[b]	32.7 ± 7.8 (38.1 %), 153.8 ± 82.7 (61.9 %)
$mPEG_{1k}$-$OPFtB_{TRI}$	-5.0 ± 0.1	11.1 ± 2.8 (99.7 %)
$mPEG_{2k}$-$OPFtB_{TRI}$	-5.3 ± 0.1	11.8 ± 3.6 (99.8 %)
$mPEG_{1k}$F13	-6.3 ± 0.1	11.9 ± 1.3 (99.9 %)
$mPEG_{2k}$DSPE	-4.9 ± 0.2	13.9 ± 1.6

Table 1: CMC values determined by surface tension using the Wilhelmy method. [a]Particle sizes of semifluorinated polymer measured by DLS as determined by volume. Data is given with the standard deviation. Each measurement was performed above the measured CMC (10 mM) and was repeated three times (n = 3). (%) signifies the percent of total particles of that particular size by volume. [b]N/A signifies that no CMC value could be determined since no constant minimum surface tension could be achieved. $mPEG_{2k}$DSPE is present as a reference compound.

The DLS further indicated that the $mPEG_x$-$OPFtB_{MONO}$ polymers did not form micelles in aqueous solution, as the particles were large and multimodal in size and had wide size distributions. Aggregate shape could not be determined; however, the DLS measurements suggested that the particles are irregular and most likely transient. In contrast, the DLS measurements of the $mPEG_x$-$OPFtB_{TRI}$ polymers indicated the formation of stable micelles, approximately 12 nm in size, which was not affected by mPEG length. (It is important to reemphasize that this size is within range to utilize the EPR effect to increase accumulation at cancerous tissue.) This behavior and size was very similar to its linear counterpart, $mPEG_{1k}$F13, where F13 corresponds to a linear PFC consisting of 13 PFC units, which had previously been synthesized by our laboratory.[36]

Due to the great deviation from a typical linear tail structure it was important to confirm the shape of the $mPEG_x$-$OPFtB_{TRI}$ polymer assemblies. Other polymer series, $mPEG_x$-$OPFtB_{MONO}$ and $mPEG_x$-$OPFtB_{DI}$, were not analysed due to random aggregation and impurity, respectively. TEM images were imaged in an aqueous solvent; however, due to the highly solvated mPEG corona and the small fluorinated core, there was little to no contrast between the vitrified water and the hydrated particles.[37] Negative staining methods were equally unsuccessful due to particle-particle aggregation. Therefore, an aqueous solution of $mPEG_{1k}$-$OPFtB_{TRI}$ polymer was blotted onto a grid and quickly dried. Although the dried assemblies may deviate in size from those present in aqueous conditions, the dried TEM image (see supplementary information) showed that the stable assemblies were spherical in shape, which corroborates the DLS data..

The collective data suggests that despite the deviation in tail structure, these polymers can form stable, spherical micelles. This behavior indicates that these amphiphiles are effective surfactants, which could serve as emulsifiers and could form stable drug-delivery vehicles if an intermediate hydrocarbon segment were installed in the polymer design.

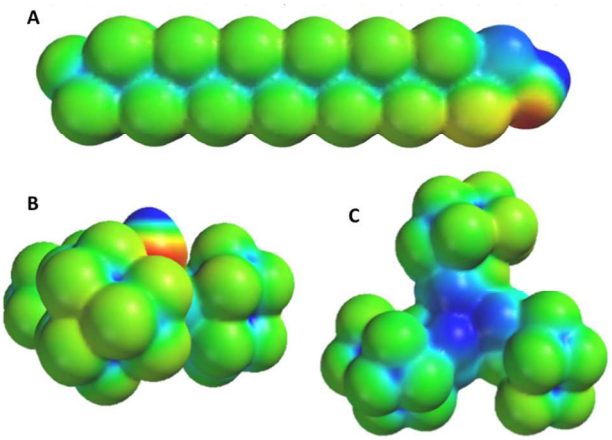

Figure 1: 6-31G** electrostatic potential surfaces calculated with SPARTAN'10 software of A: Side-on view of linear F13 alcohol, B.: PFtB-OH side-on view, and C: back-face view of PFtB-OH opposite the hydroxyl group. Values range from +150 kcal/mol to -150 kcal/mol, with red and blue signifying a value greater than or equal to the maximum in negative potential and positive potential, respectively.

To further investigate the distinct structure and subsequent physicochemical properties of the PFtB group, a calculation of the electrostatic potential energy surface (EPS) of both the $PFtB_{TRI}$-OH and the F13-OH was performed using the

SPARTAN'10 program package, **Figure 1**. These calculations showed the difference in electrostatic properties and molecular shape between the $PFtB_{TRI}$ and the linear F13 groups. The surface of the $PFtB_{TRI}$ alcohol appeared to be disk-shaped in contrast to the rod-shaped F13 alcohol. This disk orientation may allow for a more compact and viscous core, despite the relatively large steric bulk, leading to smaller micelles than one may have anticipated. The microviscosity of the micelle core of both the $mPEG_{1k}$-$OPFtB_{TRI}$ and the $mPEG_{1k}F13$ were measured via fluorescence measurements of an encapsulated P3P dye. Other polymer series were not measured as they did not form discrete and stable micelle assemblies. The microviscosity measures the ratio of the fluorescence intensity of the monomer and the eximer of an encapsulated dye. Higher microviscosity, or higher intensities of the monomer to eximer, results from a reduced mobility of the encapsulated probe and therefore indicates a more crystalline environment. Again $mPEG_{2k}DSPE$ was analysed as a reference compound. In comparison to the linear $mPEG_{1k}F13$ polymer, the $PFtB_{TRI}$ polymer had a significantly higher microviscosity, **Table 2**. The bulky $PFtB_{TRI}$ disks appear to provide increased entanglement of the unimers to increase microviscosity in comparison to the linear tail of the $mPEG_{1k}F13$.

Microviscosity of semifluorinated polymers	
$mPEG_{1k}$-$OPFtB_{TRI}$	5.2 ± 0.4
$mPEG_{1k}F13$	3.4 ± 0.2
$mPEG_{2k}DSPE$	5.6 ± 0.2

Table 2: Microviscosity of the polymer micelles was determined by fluorescence measurements of encapsulated P3P dye with error reported as STD. Higher values indicate higher microviscosity of the micelle core. $mPEG_{2k}DSPE$ is present as a reference compound.

Previous work with the $mPEG_{1K}F13$ polymer[38] demonstrated a unique ability of semifluorinated polymers to emulsify volatile fluorinated anesthetics. Stable emulsions of these anesthetics can be administered intravenously and have the potential to increase safety and reduce cost of anesthesia. The similarity in micelle behavior between $mPEG_{1K}F13$ and the $mPEG_x$-$OPFtB_{TRI}$ polymers was thought to extend also to their emulsion behaviour. A 20 % (v/v) sevoflurane emulsion with 10 % (v/v) PFOB was prepared in the same manner as with previous $mPEG_{1K}F13$ emulsions. The droplet size was measured over time and the Ostwald ripening rate monitored. **Figure 2** demonstrates that both $PFtB_{MONO}$ and $PFtB_{TRI}$ were able to form emulsions with high concentrations of fluorous anesthetics, yet only the latter was able to stabilize the particles over time. $PFtB_{MONO}$ polymer-stabilized emulsion particles grew rapidly and led to phase separation within 3 - 42 days, depending on mPEG length, while $PFtB_{TRI}$ polymers maintained small droplet sizes and were more stable than their $PFtB_{MONO}$ counterparts by at least 2 weeks. There was also dependence on the mPEG length of the polymer, where $mPEG_{2k}$-OPFtB polymers had smaller initial droplet sizes and were more resistant to phase separation. This is a crucial factor for intravenous delivery applications and for practical product shelf life. The successful emulsification of sevoflurane by $PFtB_{TRI}$ polymers again demonstrates that despite the large structural differences between the linear F13 tail and the $PFtB_{TRI}$ tail, both the branched and linear polymers have very similar surfactant behavior.

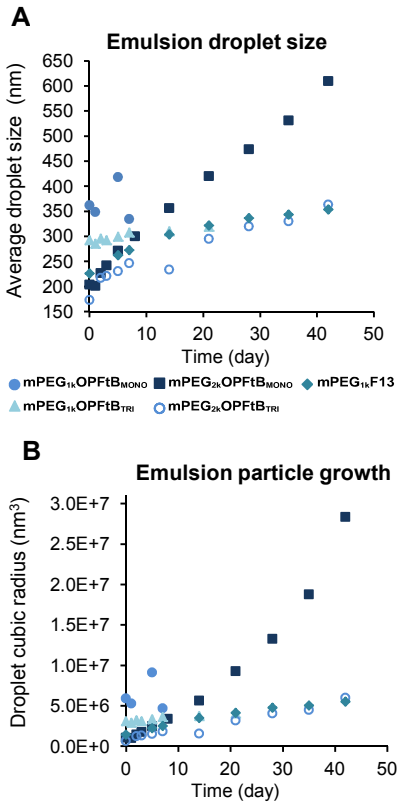

Figure 2 A: Plot of emulsion droplet size over time as measured by DLS. **B**: Plot of emulsion droplet size growth over time as measured by DLS. Linear growth of the cubic radius of the droplet over time indicates the droplets are undergoing Ostwald ripening. Note that not all polymers were measured over 50 days due to phase separation.

Since these types of polymers have been shown to be efficient surfactants their preliminary biocompatibility was investigated by performing a hemolysis assay against rabbit red blood cells. Potent surfactants have the potential to disrupt the cell membrane and lyse the cell. Two representative polymers, $mPEG_{1k}$-$OPFtB_{MONO}$ and $mPEG_{1k}$-$OPFtB_{TRI}$ were exposed at 0.1, 1, and 10 mM over 3 hrs. The polymers demonstrated less than 5 % lysis in comparison to the positive control of Milli-Q water. This demonstrates that these polymers are hemolytically safe and therefore are not restricted from further *in vitro* or *in vivo* applications.

^{19}F-MR imaging characterization. With the surfactant capabilities of the $mPEG_x$-$OPFtB_{TRI}$ well established, the function of the fluorous tail as a ^{19}F-MRI contrast agent was investigated. For optimal signal intensity, the $mPEG_{1k}$-$OPFtB_{TRI}$ polymer was solely chosen for analysis, as this compound has the highest percent fluorine per molecule of the series and exhibits the best physico-chemical nanoparticle characteristics. Preliminary relaxivity measurements in D_2O at 9.4 T showed that these polymers have one single, narrow ^{19}F resonance at -70 ppm, and a half-width of approximately 25 Hz,

arising from 27 equivalent ^{19}F atoms per molecule. These polymers also exhibited short T_1 values that provide quick recovery, increased scan efficiency for spin-density weighted images and show relatively long T_2 values that predict minimal decay in signal intensity over that scan time, **Table 3**. The characteristics of the $mPEG_x$-$OPFtB_{TRI}$ polymers is in stark contrast with the $mPEG_{1k}F13$ polymer, which as an aqueous assembly exhibits six ^{19}F signals that are extremely broadened to the point of almost complete signal nullification. In total, these results indicated that the $mPEG_x$-$OPFtB_{TRI}$ polymers could feasibly serve as effective ^{19}F-MRI contrast agents due to their short T_1 times and single ^{19}F resonance, removing the need for spectroscopic imaging techniques.

Polymer	T_1 (s)	T_2 (s)
$mPEG_{1k}$-$OPFtB_{TRI}$	0.53 ± 0.01	0.11 ± 0.01
$mPEG_{2k}$-$OPFtB_{TRI}$	0.49 ± 0.01	0.11 ± 0.01

Table 3: ^{19}F relaxivity measurements in D_2O at 9.4 T. $PFtB_{TRI}$ polymers exhibit ^{19}F-NMR characteristics amenable to ^{19}F-MR imaging: a single ^{19}F resonance, short T_1 values and relatively long T_2 values.

The mPEG length had little effect on the T_2 values, indicating that both polymer tails had similar degrees of mobility. This enhanced mobility in comparison to linear fluorous tails in aqueous self-assemblies suggested that the non-linear structure of the PFtB group allows for enhanced mobility of the fluorous tail.[25] High mobility of the PFtB group in the assembled micelle is not in conflict with the microviscosity measurements discussed previously. The increased viscosity of the $mPEG_{1k}$-$OPFtB_{TRI}$ micelle core in comparison to the linear $mPEG_{1k}F13$ micelle core was hypothesized to derive from restricted dynamics of the entire unimer rather than the fluorous tail itself. Mobility of the PFtB group has been shown to be maintained even in crowded environments such as lipid-membrane bound states.[32] In the self-assembly these bulky fluorous tails exhibit adequate mobility, which is characteristic of a fluorous domain, and therefore maintain high signal intensity for NMR applications.

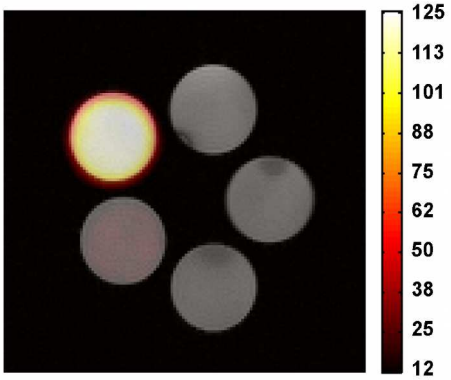

Figure 3: ^{19}F-MR phantom images superimposed upon ^{1}H MR images of $mPEG_{1k}$-$OPFtB_{TRI}$ polymer solutions in Milipore water, with 25 min scan time, at 4.7 TF and scaled according to SNR. From top center moving counter clock-wise: Blank (0 mM), 5 mM, 1 mM, 0.1 mM, and 0.01 mM. The 5 mM phantom shows strong signal while 1 mM demonstrates the limit of detectability.

After these successful preliminary relaxivity measurements, the $mPEG_{1k}$-$OPFtB_{TRI}$ phantoms, ranging in concentration from 0.01 mM to 5 mM, were imaged at 4.7 T. These polymer solution images in **Figure 3** show molecular ^{19}F images overlaid upon anatomical ^{1}H images. SNR was sufficient even at a molecular concentration of 1 mM, corresponding to a ^{19}F concentration of 27 mM, a reasonable concentration for *in vivo* accumulation of the labeled polymer considering the low field strength and lack of sensitizers or signal enhancing sequences. SNR could potentially be augmented with more efficient pulse sequences[39] or higher field strengths. Further investigation of these polymers is currently underway to elucidate their *in vivo* properties, including toxicity, bioaccumulation, and biodistribution via ^{19}F-MR imaging.

Conclusions

Semifluorinated surfactants with bulky PFtB tails have been prepared and shown to self-assemble into small, discrete, spherical micelles in aqueous solution. The $PFtB_{TRI}$ polymers and their linear counterpart, $mPEG_{1K}F13$, both assemble into spherical micelles approximately 12 nm in size. However, the $PFtB_{TRI}$ polymer has a microviscosity that is approximately 1.5 times that of the linear $mPEG_{1k}F13$. Although both polymers have the same mPEG length and the same number of fluorine atoms in their tail, the disk shape of the $PFtB_{TRI}$ tail appears to allow for an alternative packing of unimers in the micelle, resulting in a highly viscous core. The $mPEG_x$-$OPFtB_{TRI}$ polymers were also able to stably emulsify 20 % (v/v) sevoflurane with 10 % (v/v) PFOB as an additive. This further demonstrates that despite the distinct tail structure, these polymers are effective surfactants.

PFtB fluorous tails not only engender stable self-assembly but may also serve as a ^{19}F-MRI contrast agents. $PFtB_{TRI}$ polymer micelles gave rise to a single, narrow ^{19}F-NMR signal in D_2O. These assemblies exhibit short T_1 and long T_2 values demonstrating their potential towards ^{19}F-MR imaging. Polymer phantoms show effective contrast as low as 1 mM molecular concentration, corresponding to 27 mM fluorine concentration. This preliminary data demonstrates the multifunctional utility of the PFtB fluorous tail as both a stabilizing force in the self-assembly and a ^{19}F-MRI label, and therefore its potential in theranostic therapy. Future work will modulate the polymer design to include a small hydrocarbon segment to allow for encapsulation of hydrophobic molecules, such as anti-cancer agents and antimicrobials.

Acknowledgements

The research described in this article was partially supported by the National Institutes of Health (grant # GM079375 to SM) and by the University of Wisconsin-Madison School of Pharmacy. We thank Dr. Jeremy Gordon and the Wisconsin Institutes for Medical Research (WIMR) Imaging Sciences Center for help with ^{19}F imaging. The authors gratefully acknowledge use of facilities and instrumentation supported by

the NSF-funded University of Wisconsin Materials Research Science and Engineering Center (DMR-1121288), and the Small Molecule Screening and Synthesis Facility in the University of Wisconsin Carbone Cancer Center. We also thank Prof. Jamey Weichert, Prof. Glen Kwon, and William Tucker for helpful discussions.

Notes and references

[1] Torchilin, V. P. *J. Controlled Release* **2001**, *73*, 137-172.
[2] Skrabania, K.; Laschewsky, A.; Berlepsch, H. v.; Bottcher, C. *Langmuir* **2009**, *25*, 7594-7601.
[3] Yoon, H. J.; Jang, W. D. *J. Mater Chem*. **2010,** *20*, 211–222.
[4] Fernandez, A. M.; Van Derpoorten, K.; Dasnois, L.; *J. Med. Chem*. **2001**, *44*, 3750 - 3753.
[5] Singh, S.; Dash, A. K. *Crit. Rev. Ther. Drug Carrier Syst*. **2009**, *26*, 333–372.
[6] Maeda, H.; Sawa, T.; Konno, T. *J. Controlled Release* **2001**, *74*, 47-61.
[7] Torchilin, V. P. *Pharm. Res.* **2007**, *24*, 1-16.
[8] Chen, H.; Kim, S.; He, W.; Wang, H.; Low, P.S.; Park, K.; Chang, J.-X. *Langmuir*, **2008**, *24*, 5213-5217.
[9] Jee, J.-P.; McCoy, A.; Mecozzi, S. *Pharm. Res.* **2012**, *29*, 69-82.
[10] Gindy, M. E.; Prud'homme, R. K. *Exp. Opin. Drug Deliv*. **2009**, *6*, 865-878.
[11] Cametti, M.; Crousse, B.; Metrangolo, P.; Milani, R.; Resnati, G. *Chem. Soc. Rev*. **2012**, *41*, 31-42.
[12] Tran, T. D.; Caruthers, S. D.; Hughes, M.; Marsh, J. N.; Cyrus, T.; Winter, P. M.; Neubauer, A. M.; Wickline, S. A.; Lanza, G. M.; *Int. J. Nanomed*. **2007**, *2,* 515–526.
[13] Wahajuddin; Arora, S. *Int. J. Nanomed.* **2012**, *7*, 3445-3471.
[14] Idée, J.-M.; Port, M.; Medina, C.; Lancelot, E.; Fayoux, E.; Ballet, S.; Corot, C. *Toxicology* **2008**, *248*, 77-88.
[15] Ruiz-Cabello, J.; Barnett, B. P.; Bottomley, P. A.; Bulte, J. W. M. *NMR Biomed.* **2011**, *24*, 114-129.
[16] Lanza, G. M.; Winter, P. M.; Neubauer, A. M.; Caruthers, S. D.; Hockett, F. D.; Wickline, S. A. *Curr. Top. Dev. Biol.* **2005**, *70*, 57–76.
[17] Janjic, J. M.; Srinivas, M.; Kadayakkara, D. K. K.; Ahrens, E. T. *J. Am. Chem. Soc*. **2008**, *130*, 2832–2841.
[18] Patrick, M. J.; Janjic, J. M.; Teng, H.; O'Hear, M. R.; Brown, C. W.; Stokum, J. A.; Schmidt, B. F.; Ahrens, E. T.; Waggoner; A. S. *J. Am. Chem. Soc*. **2013**, *135*, 18445-18457.
[19] Soman, N. R.; Lanza, G. M.; Heuser, J. M.; Schlesinger, P. H.; Wickline, S. A. *Nano Letters* **2008**, *8*, 1131-1136.
[20] Díaz-López, R.; Tsapis, N; Fattal, E. *Pharmaceutical Research* **2010**, *27,* 1-16.
[21] Yu, J.-X.; Kodibagkar, V. D.; Cui, W.; Mason, R. P. *Curr. Med. Chem.* **2005**, *12*, 819–848.
[22] A. M. Nyström, J. W. Bartels, W. Du and K. L. Wooley, J. Polym. Sci., Part A: Polym. Chem., **2009**, *47*, 1023–1037.
[23] H. Peng, I. Blakey, B. Dargaville, F. Rasoul, S. Rose and A. K. Whittaker, Biomacromolecules, **2009**, *10*, 374–381.
[24] Nurmi L.; Peng, H.; Seppälä, J.; Haddleton, D. M.; Blakey, I.; Whittaker, A. K., *Polym. Chem.* **2010**, *1*, 1039-1047.
[25] Du, W.; Nyström, A. M; Zhang, L.; Powell, K. T.; Li, Y.; Cheng, C.; Wickline, S. A.; Wooley, K. L. *Biomacromolecules* **2008**, *9*, 2826–2833.
[26] Jiang, Z.-X.; Liu, X.; Jeong, E. K.; Yu, Y. B. *Angew. Chem. Int. Ed.* **2009**, *48*, 4755-4758.
[27] Torchilin, V. P. *AAPS Journal* **2007**, *9*, E128-E147.
[28] Porsch, C.; Zhang, Y.; Östlund, Å.; Damberg, P.; Ducani, C.; Malmström, E.; Nyström, A. M *Part. Part. Syst. Charact.* **2013**, 30, 381–390.
[29] Du, W.; Xu, Z.; Nyström, A. M.; Zhang, K.; Leonard, J. R.; Wooley, K. L. *Bioconjugate Chem.* **2008**, *19*, 2492–2498.
[30] Richardson, J. C.; Bowtell, R. W.; Maeder, K.; Melia, C. D. *Adv. Drug Delivery Rev.* **2005**, *57*, 1191–1209.
[31] Szabó, D.; Mohl, J.; Báint, A.-M.; Bodor, A.; Rábai, J. *J. Fluor. Chem.* **2006**, *127*, 1496-1504.
[32] Nemes, A.; Tölgyesi, L; Bodor, A.; Rábai, J.; Szabó, D. *J. Fluor. Chem.* **2010**, *131*, 1368-1376.
[33] Buer, B. C.; Levina, B. J.; Marsh, E. N. G. *J. Pept. Sci*. **2013**, *19*, 308–314.
[34] a) Jiang, Z.-X.; Yu, Y. B. *Tetrahedron* **2007**, *63*, 3982–3988. b) Jiang, Z.-X.; Yu, Y. B. *Synthesis* **2008**, 215–220. c) Jiang, Z.-X.; Liu, X.; Jeong, E. K.; Yu, Y. B. *Angew. Chem. Int. Ed.* **2009**, *48*, 4755-4758.
[35] Weissig, V.; Whiteman, K.R.; Torchilin, V.P. *Pharm. Res.*, **1998**, *15*, 1552-1556.
[36] Parlato, M. C.; Jee, J.-P.; Teshite, M.; Mecozzi, S. *J. Org. Chem.* **2011**, *76*, 6584-6591.
[37] Johansson, E.; Lundquist, A.; Zuo, S.; Edwards, K. *Biochimica et Biophysica Acta* **2007**, *1768,* 1518-1525.
[38] Fast, J. P.; Perkins, M. G.; Pearce, R. A.; Mecozzi, S. *Anesthesiology* **2008**, *109*, 651-656.
[39] Ruiz-Cabello, J.; Barnett, B. P.; Bottomley, P. A.; Bulte, J. W. M. *NMR Biomed* **2011**, *24*, 114-129.